



A novel quantitative method for evaluating floc strength under turbulent flow conditions

Junguo He^a, Jian Liu^{a,*}, Yixing Yuan^b, Jie Zhang^b

^aSchool of Municipal and Environmental Engineering, Harbin Institute of Technology, 73 Huanghe Road, Harbin, China, email: junguohe@263.net (J. He), Tel. +86 13704803541; email: liujianhitwater@163.com (J. Liu)

^bState Key Laboratory of Urban Water Resources and Environment, School of Municipal and Environmental Engineering, Harbin Institute of Technology, 73 Huanghe Road, Harbin, China, emails: yuanyixinghit@163.com (Y. Yuan), zhangjiehitwater@163.com (J. Zhang)

Received 18 April 2014; Accepted 15 August 2014

ABSTRACT

In this paper, we established a novel quantitative method for evaluating floc strength under turbulent flow conditions. The key factors involved were the binding and breaking forces of floc. The floc's binding force was considered to be floc strength and could be described as a function of the floc diameter (d) and fractal dimension (D_f). A coefficient of binding force (k) was also developed to express the less accessible parameters, such as densities and areas. Moreover, the breaking force was proportional to the squared average velocity gradient (G) and the fourth power of d . Jar tests were conducted to test this approach using the polyaluminum chloride as the coagulant. The physical parameters involved were monitored online. A critical G value was determined to be 98.4 s^{-1} based on the variation of these parameters. Accordingly, the binding and breaking forces were calculated, and the k value was obtained as 6.621×10^{-3} . The floc strengths with various coagulant dosages were calculated and the highest floc strength was achieved at a dosage of 22.5 mg/L. This method could be used to optimize coagulation in real-world settings.

Keywords: Floc strength; Turbulent flow; Binding force; Breaking force; Fractal dimension

1. Introduction

Flocculation, which is effective in removing colloidal or suspended particles, is a key process in water treatment, due to its simple operation procedure, short production cycle, low cost, and good performance [1]. The flocculation process is usually divided into two steps. The first step is coagulation, which involves metal

ions hydrolysis, particle transport, and particle destabilization. The second step promotes agglomeration of destabilized or small particles into larger flocs [2,3]. The goal of flocculation is to increase floc size and strength, improving colloids removal, and the small particle precipitation process that follows.

Floc growth is generally moderated by floc breakage; floc form and break, balancing the floc aggregation rate. The size of flocs at steady state is governed by the shear condition within the flocculation tanks

*Corresponding author.

This article was originally published with errors. This version has been corrected. Please see Corrigendum (<http://dx.doi.org/10.1080/19443994.2015.1058548>).

[4,5]. As such, flocculation processes are generally designed to minimize floc breakage [6]. However, certain areas within flocculation tanks at drinking water treatment plants have higher shear conditions, such as the impeller zone and near weirs and ledges [5]. The flocs tend to break into smaller particles when they are subjected to the stress of a higher shear force. This presents a significant challenge downstream, because these particles cannot be effectively removed in solid–liquid separation process [7,8]. Therefore, floc strength, which is an indicator of the floc's capacity to resist shear force, plays an important role in determining flocculation performance.

Floc strength is related to the inter-particle bonds between aggregate components [9]. Hence, a floc will be broken when the shear force applied to its surface is larger than the bonding strength within the floc [10]. Strength factor, defined as the ratio of floc size after breakage to its size prior to a specific agitation rate, is the simplest way to evaluate floc strength [5,11]. To rapidly determine floc strength factor, some researchers used photometric dispersion analyzer (PDA) to monitor floc formation online, and proposed a flocculation index (FI) to surrogate the floc size [12,13]. However, it is hard to directly compare floc strengths using strength factor under various agitation conditions. Therefore, the empirical relation between the applied shear and the broken floc size was used to evaluate floc strength [14–17].

Although the strength factor and the empirical equation have been used to measure floc strength, they provide only indirectly comparison of floc strength and do not refer to quantitative studies of the floc strength. The theoretical method for floc strength evaluation was elucidated under the turbulent flow condition by Bache et al. [18]. The results showed that the average strength per unit area at the plane of rupture could be determined by water density, local rate of energy dissipation per unit mass, kinematic viscosity, and floc size. However, the calculation was conducted based on the non-porous and sphere hypothesis for floc structure. In fact, the formed flocs were highly porous with irregular structures. Previous researches considered that the morphological properties, such as floc shape and structure, could affect the aggregation behavior of particles, especially with regard to density and settling velocity [19–21]. Therefore, to achieve more accurate calculation, we must take into account the morphological properties of floc.

Jin et al. [22] established an evaluation method of floc strength using PDA online monitoring, and morphological analysis. In their study, the shear force, which was used to distinguish the critical condition of floc breakage, was derived based on a laminar flow

condition. However, all flocculation tanks are operated under the turbulent flow condition. The evaluation of floc strength under turbulent condition is critical to optimize flocculation process of the water treatment [2]. Energy spectrum, an important parameter in floc strength calculation, is computed by Kolmogoroff locally isotropic turbulence theory [11]. Accordingly, the scale of turbulence determines the energy content of an eddy. The large eddies caused by the agitation of the flocculation tank dissipate a little energy in the system, while the small eddies dissipate the large portion of energy [5].

The objectives of this study were to develop a new approach for quantitative evaluating floc strength under turbulent flow conditions and propose an experimental method for floc breakage monitoring. The binding force, which was considered to be the floc strength, was theoretically calculated using the floc's morphological characteristics. The breaking force of fluid was deduced based on the theory of Kolmogoroff locally isotropic turbulence. The experiments for determining the critical condition of floc breakage were conducted, and the strengths of polyaluminum chloride (PAC) floc under various dosages were also investigated.

2. Evaluation of floc strength

Floc strength and size are strongly influenced by the quality of coagulants and the kinetic parameters of coagulation. Under a special coagulant quality condition, the flocs strength and size are directly restricted by the kinetic parameters of coagulation. Floc diameter and strength are controlled by two counteracting forces under a given agitation condition: the floc's binding force and the turbulent breaking force of the fluid [23]. The binding force is related to the floc's morphological characteristics, and the breakage of floc is determined by turbulence kinetic parameters [24,25]. In this part, the floc's binding force and the turbulent breaking force of fluid were deduced by morphological characteristics of floc and the theory of Kolmogoroff locally isotropic turbulence, respectively. A new method for quantitative evaluating the floc strength could be developed based on the binding and the breaking forces of floc.

2.1. The binding force of floc

The binding force B_f (kg m s^{-2}) is proportional to the net section area A_n (m^2) at the rupture plane, shown as below [23]:

$$B_f = \sigma A_n \quad (1)$$

where σ is a constant reflecting average binding strength with respect to the net section area of floc ($\text{kg m}^{-1} \text{s}^{-2}$).

The net volume V_n (m^3) of a floc which derives from floc diameter d (m) is given as:

$$V_n = \alpha(1 - e)d^3 \quad (2)$$

where α is the geometry factor ($\alpha = \pi/6$) (–) and e is the floc porosity (–). Hence, the effective diameter d_e (m) which is relative to the net section area and the net section area A_n (m^2) at the plane of rupture are shown as:

$$d_e = \alpha^{1/3}(1 - e)^{1/3}d \quad (3)$$

$$A_n = \frac{\pi}{4}\alpha^{2/3}(1 - e)^{2/3}d^2 \quad (4)$$

Consequently, the binding force of floc can be derived from Eqs. (1) and (4):

$$B_f = \frac{\pi}{4}\alpha^{2/3}(1 - e)^{2/3}d^2\sigma \quad (5)$$

The e of a floc can be deduced by means of the floc density function (6) and the material balance of the floc [26].

$$\rho_e = \rho_f - \rho_w = \frac{a}{d^{k_p}} \quad (6)$$

where ρ_e is the floc effective density (kg m^{-3}); ρ_f and ρ_w are the densities of floc and water, respectively (kg m^{-3}); and a and k_p are density function coefficients, (kg m^{-3}) and (–).

The material balance of the floc is:

$$\rho_f V_f = \rho_w V_w + \rho_0 V_0 \quad (7)$$

where ρ_0 is the density of primary particle (kg m^{-3}); V_f is the volume of floc (m^3); V_w is the volume of water in floc which can be established as eV_f (m^3); and V_0 is the volume of primary particles in floc, written as $(1 - e)V_f$ (m^3). Therefore, Eq. (7) can be written as:

$$\rho_f V_f = \rho_w eV_f + \rho_0(1 - e)V_f \quad (8)$$

By substituting Eq. (6) into Eq. (8), the following can be obtained that:

$$1 - e = \frac{a}{(\rho_0 - \rho_w)d^{k_p}} \quad (9)$$

From Eqs. (5) and (9), the binding force of floc is shown as:

$$B_f = \frac{\pi^{5/3}a^{2/3}\sigma}{48^{2/3}(\rho_0 - \rho_w)^{2/3}}d^{(2-2k_p/3)} \quad (10)$$

In addition, flocs formed during coagulation and flocculation process have a fractal characteristic [20], and the mass of floc M (kg) is in contact with the fractal dimension D_f (–) [21,24]:

$$M = k_1 d^{D_f} \quad (11)$$

where k_1 is a coefficient. Meanwhile, the M can be written in the following form as:

$$M = \rho_e V_n \quad (12)$$

Therefore, by substituting Eqs. (2), (6), and (9) into Eq. (12), the following equation can be obtained:

$$M = \frac{\pi a^2}{6(\rho_0 - \rho_w)}d^{3-2k_p} \quad (13)$$

Assuming $k_2 = 6^{-1}\pi a^2 (\rho_0 - \rho_w)^{-1}$ and k_2 is a coefficient.

$$M = k_2 d^{3-2k_p} \quad (14)$$

Comparing Eq. (11) with Eq. (14), the following equation can be obtained:

$$D_f = 3 - 2k_p \quad (15)$$

Eqs. (6) and (15) show that floc fractal dimension is proportional to floc density. This is consistent with the conclusion that fractal dimension can be used to describe floc structure characteristics and density [21,27]. The relationship between fractal dimension and density is shown in Eq. (15). When the two-dimensional or three-dimensional fractal dimension of floc is obtained by imaging analysis, floc density can be directly calculated, and the quantitative relation of the particles' settling character can be determined.

Substituting Eq. (15) into Eq. (10), the binding force of floc is:

$$B_f = \frac{\pi^{5/3} a^{2/3} \sigma}{48^{2/3} (\rho_0 - \rho_w)^{2/3}} d^{(1+D_f/3)} \quad (16)$$

Under similar water quality and flocculation conditions, a , σ , and $(\rho_0 - \rho_w)$ can be considered to be constants [23]. Then, the binding force of floc can be written as:

$$B_f = kd^{(1+D_f/3)} \quad (17)$$

where k is the coefficient of binding force and $k = 48^{-2/3} \pi^{5/3} a^{2/3} \sigma (\rho_0 - \rho_w)^{-2/3}$. Eq. (17) shows that the floc's binding force is a function of floc diameter and fractal dimension. When floc size is the same, as the fractal dimension increases, the floc becomes more compact and the binding force increases. Moreover, while the fractal dimension remains unchanged, the binding force of floc is improved due to the net section area of floc and the numbers of inter-particle bonds are increased as the floc size is enhanced.

2.2. The turbulent breaking force of fluid

Turbulent motions in flocculation tank prevent floc growth. These motions produce an external breaking force, destroying the floc [23]. The difference of the pressures Δf ($\text{kg m}^{-1} \text{s}^{-2}$) between two adjacent points at a small distance is considered to be the external breaking force exerted on floc by micro-turbulent eddies. This is shown as [25]:

$$\Delta f = |\overline{p_1 - p_2}| = \rho_w |\overline{v_1 - v_2}|^2 \quad (18)$$

where p_1 and p_2 are the pressures at the adjacent point 1 and 2 at a small distance, respectively ($\text{kg m}^{-1} \text{s}^{-2}$); $|\overline{p_1 - p_2}|$ is the absolute value of the mean difference between the above two pressures ($\text{kg m}^{-1} \text{s}^{-2}$); v_1 and v_2 are the fluctuation velocities of the water at points separated from each other by a small distance (m s^{-1}); and $|\overline{v_1 - v_2}|$ is the absolute value of the mean difference between the two velocities (m s^{-1}).

There are many expressions to describe the value of $|\overline{v_1 - v_2}|$, which depend on the scale of the motion under consideration. Usually, the motion scale is determined by the Kolmogoroff micro-scale λ (m), a particular length scale, defined as [25]:

$$\lambda = (v^3/\varepsilon)^{1/4} \quad (19)$$

where v is the kinematic viscosity ($\text{m}^2 \text{s}^{-1}$) and ε is the mean rate of energy dissipation per unit volume ($\text{J m}^{-3} \text{s}^{-1}$).

Under the theory of Kolmogoroff locally isotropic turbulence, the value of $|\overline{v_1 - v_2}|$ is [23]:

$$|\overline{v_1 - v_2}| = \beta(\varepsilon d/\rho_w)^{1/3} d \gg \lambda \text{ (inertia area)} \quad (20)$$

$$|\overline{v_1 - v_2}| = \gamma\sqrt{\varepsilon/\mu} d \ll \lambda \text{ (viscous area)} \quad (21)$$

where μ is the absolute viscosity ($\text{kg m}^{-1} \text{s}^{-1}$); β and γ are the constants with values approximately 1 and $15^{-0.5}$, respectively.

Substituting Eqs. (20) and (21) into Eq. (18), the pressure difference can be shown as:

$$\Delta f = \rho_w^{1/3} \varepsilon^{2/3} d^{2/3} d \gg \lambda \text{ (inertia area)} \quad (22)$$

$$\Delta f = \frac{\rho_w \varepsilon}{15\mu} d^2 d \ll \lambda \text{ (viscous area)} \quad (23)$$

Therefore, the breaking force of fluid F (kg m s^{-2}) can be determined by multiplying surface area of the floc into Eqs. (22) and (23), and it is shown as:

$$F = (\pi \rho_w^{1/3} \varepsilon^{2/3} d^{8/3})/4 d \gg \lambda \text{ (inertia area)} \quad (24)$$

$$F = \frac{\pi \rho_w \varepsilon}{60\mu} d^4 d \ll \lambda \text{ (viscous area)} \quad (25)$$

In real flocculation processes, floc breakage often occurs in viscous areas [5,28]. Hence, Eq. (25) shows the breaking force of the fluid.

It can be known from previous research [5,29]:

$$G = \sqrt{\varepsilon/\mu} \quad (26)$$

$$\varepsilon = (\rho_w P_0 N^3 D^5)/V \quad (27)$$

where G is the average velocity gradient (s^{-1}), P_0 is the impeller power number (-), N is the impeller speed (rps), D is the impeller diameter (m), and V is the stirred tank volume (m^3). By substituting Eq. (26) into Eq. (25), the turbulent flow breaking force is:

$$F = \frac{\pi \rho_w}{60} d^4 G^2 \quad (28)$$

Eq. (28) shows that the turbulent breaking force of fluid is proportional to the squared average velocity gradient and the fourth power of floc diameter. The turbulent breaking force of fluid increases with an increasing G

value when floc size remains the same. Therefore, the higher the shear strength, the more likely the floc is to break. On the other hand, when the G value is unchanged, the area of floc resisting the shear force increases rapidly as the floc size increases. Thus, the larger floc is more prone to breaking into small particles.

2.3. The strength of floc

In this study, floc strength can be directly calculated by evaluating the floc's binding force. Under a given agitation condition, the critical condition of floc breakage is considered to be the binding force equal to the breaking force, which has following form:

$$B_f = F \quad (29)$$

After the growth phase of floc, floc size and fractal dimension remain stable and the floc strength no longer changes. When the broken shear force is lower, breaking force is less than binding force and the floc will remain stable. The turbulent breaking force of fluid increases dramatically with the rising of shear force. When binding force is equal to breaking force, the critical condition of floc breakage is reached, leading to floc breakage.

To investigate the critical condition of floc breakage, we applied increased agitation rates to grown floc to cause floc breakage. The critical condition can be obtained by online monitoring of the variation of the floc diameter, fractal dimension, and particle size distribution, which are realized by the laser light scattering technology. When G , d , and D_f have been obtained by experiments, the floc strength and the coefficient k can be calculated by Eqs. (28) and (17), respectively.

3. Materials and experimental methods

3.1. Raw water and coagulant

Kaolin was used as the model suspension in this study. The stock suspensions were prepared by dispersing 250 g of kaolin in 1L of distilled water at high-shear condition (500 rpm), and then allowing it to settle for 30 min. After settlement, the solution pH was adjusted to 7.50 ± 0.05 with 0.1 mol/L NaOH. The blending suspension was then settled for 24 h. The experimental suspension (40 mg/L) was prepared by diluting the stock suspension with distilled water. In addition, the pH value was kept at 7.50 ± 0.05 by adding 0.1 mol/L HCl or NaOH.

PAC (analytic reagent) was used as the coagulant and 0.1 mol/L alum solutions were prepared with deionized water as the experimental solution.

3.2. Jar test

Coagulation experiments were performed in a jar test apparatus (MY3000, Wuhan MeiYu Instrument Co. Ltd, China) at a room temperature of $20 \pm 1^\circ\text{C}$. Water samples (1L) were placed on the jar tester under the following conditions: rapid stirring (150 rpm) for 1 min with PAC dose, followed by slow stirring (40 rpm) for 20 min, and settled for 30 min. When coagulation was complete, the supernate (50 mL) was collected to measure residual turbidity. Turbidity and Zeta potential were measured using a turbidimeter (2100P, Hach Co., US) and a zetasizer (Zetasizer2000, Malvern, UK), respectively.

To investigate the critical condition of floc breakup and calculate floc strength, different shear forces were applied to the grown flocs to cause breakage when slow stirring was finished at an optimum coagulant dosage. Increased shear rates of 40 (14.9 s^{-1}), 80 (42.2 s^{-1}), 120 (77.5 s^{-1}), 160 (119.3 s^{-1}), 200 (166.7 s^{-1}), and 240 (219.1 s^{-1}) rpm were applied for an additional 5 min sequentially (average velocity gradients, calculated from Eqs. (26) to (27), in brackets).

3.3. Floc size and fractal dimension

The dynamic floc diameter of the flocculate and break-up process were monitored online using a particle size distribution analyzer (Mastersizer 2000, Malvern Instruments, UK) [19,30]. When the water sample in the cylindrical jar was drawn through the instrument by a peristaltic pump at a flow rate of 2.0 L/h [8], the floc diameter was measured by the optical unit of the instrument, and then the tested sample was returned to the jar tester. Floc size distribution after breakage was immediately monitored by the particle size distribution analyzer [31,32]. The floc diameter was denoted by the mean size of the floc ($d_{0.5}$) [1].

The floc fractal dimension detected using a particle size distribution analyzer. When the laser light beam passed through the water sample, the light intensity scattered by the flocs was proportional to the particle size. Large flocs scattered at lower angles, while small flocs scattered at higher angles. The relationship between scatter angle and the scatter wave vector follows a law expressed through the following Eq. [30]:

$$Q = \frac{4\pi n \sin(\theta/2)}{\lambda_0} \quad (30)$$

where Q is the scatter wave vector, n is the refractive index of the medium, θ is the scatter angle, and λ_0 is the laser light wavelength in vacuum. The light intensity I , which can be described by the fractal dimension, is defined using the following Eq. [33]:

$$I \propto Q^{-D_f} \quad (31)$$

Thus, there is a linear relationship between the light intensity and the scatter wave vector on a log–log plot, and D_f could be derived as the slope of the line.

3.4. Floc strength

As previously noted, binding force was used to determine floc strength in this study. Once we obtained the floc diameter d and the average velocity gradient G at the critical breaking point, floc strength could be calculated using Eq. (28) above and the coefficient k could be calculated using Eq. (17).

4. Experimental results and discussion

4.1. Coagulation optimization

Turbidity removal efficiency and Zeta potential variation were investigated using various PAC dosages. As shown in Fig. 1, turbidity removal and Zeta potential variation correlated well with coagulant dose. Zeta potential increased dramatically with PAC dosage in the range of 0–5 mg/L; the rate of increase

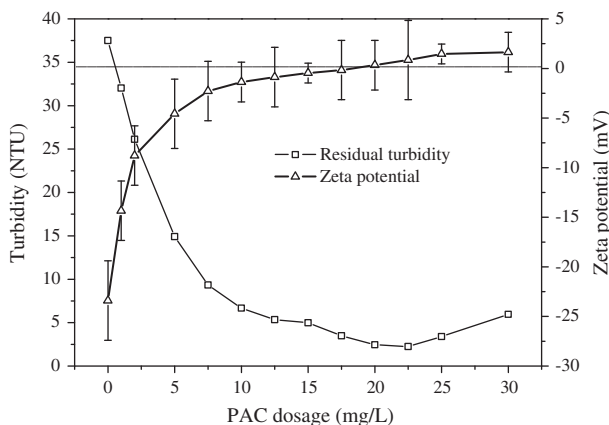


Fig. 1. Effect of PAC dosage on residual turbidity and Zeta potential.

declined from the dosage of 7.5–22.5 mg/L. Once the dosage was higher than 22.5 mg/L, a plateau was achieved on the Zeta potential curve. At the lower coagulant dose range, residual turbidity decreased rapidly; when coagulant dose was increased from 10 to 22.5 mg/L, turbidity removal was gradually increased. However, at the higher PAC dosage, the turbidity removal decreased. Therefore, the PAC dose of 22.5 mg/L was the most efficient coagulant dosage in terms of turbidity removal.

4.2. Online monitoring results of the floc breakage

4.2.1. Variation of floc diameter

Floc size variation in the formation and breakage phases reflects the of colloidal particle evolution. The profiles of floc size during the growth process and the breakage stage were shown as Fig. 2.

There were three phases in the floc formation process: lag phase, swift growth phase, and steady state phase. In the lag phase, coagulants were fully mixed with the water sample, and began to contact the initial particles. Floc size did not appear to increase in this phase. The flocculation curves demonstrated that floc size increased remarkably in the swift growth phase. The negative charge on the surface of initial particles was strongly neutralized by PAC with a highly positive charge; the particles then collided with each other, resulting in larger flocs [19]. Moreover, the bridge and sweep characteristics of PAC could combine small particles into a larger floc, causing an increase in floc size. The steady-state phase, generally regarded as a balance between floc growth and breakage under a given shear condition, was achieved after slow stirring

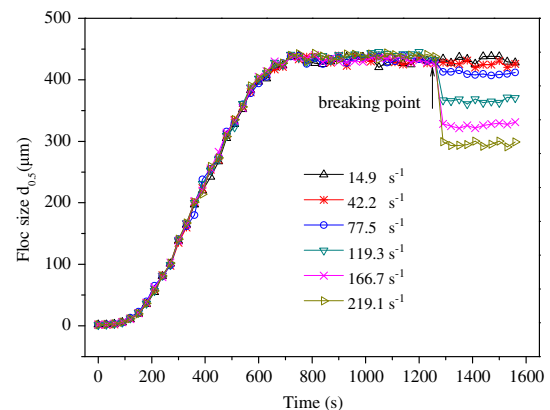


Fig. 2. Variation of floc size in formation and breakage phases with different breakage shear forces.

for a few minutes. The floc size no longer increased in this phase. The durations of the lag stage and the swift growth phase, directly obtained from the flocculation curve, were 150s and 480s, respectively; the floc size was 431 μm in steady-state phase.

After the first plateau, the flocs were exposed to strong shear force with various G values to determine the critical condition of floc breakage. The stirring rate during the breakage process greatly influenced floc size; the variation of the floc size with different breakage times was shown as Fig. 2. Overall, floc size decreased with increasing breakage shear forces. The floc size seldom varied when the G value was increased from 14.9 to 42.2 s^{-1} . There was only a slight reduction of floc size when the G value was 77.5 s^{-1} .

These results indicated that the floc had not been broken or had been only slightly broken at a low stirring rate. However, when the G value was 119.3 s^{-1} , or higher than 166.7 s^{-1} , the floc size was considerably reduced immediately after introducing increased shear. These results were consistent with Yu et al. [34], who studied Al-humic flocs breakage. That research noted that FI values strongly correlated with floc size decreased with increased stirring speeds.

4.2.2. Effect of shear force on fractal dimension

As shown in Eq. (31), when the light intensity I was plotted on a log–log scale against the scatter wave vector Q , the fractal dimension D_f could be easily obtained. Values of D_f , investigated to analyze floc structure, were calculated after increasing stirring speed. The results were shown as Fig. 3, which showed an increasing in the D_f value as the G value

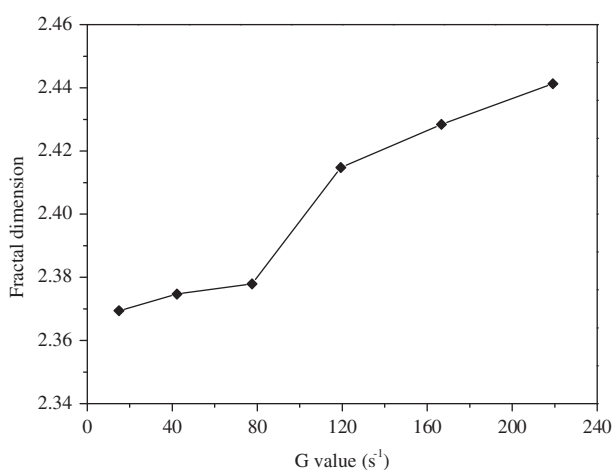


Fig. 3. Variation of fractal dimension after breakage with different G .

increased from 14.9 to 219.1 s^{-1} . By a low breaking shear, D_f varied little with different G values in the range of 14.9–77.5 s^{-1} . This showed that PAC flocs were insensitive to the shear condition changes at lower G value due to the major coagulation mechanisms of charge neutralization, sweep, and bridge. D_f clearly increased when G was above 119.3 s^{-1} . This indicated that high stirring rate might accelerate floc breakage.

The flocs achieving size balance had a branched structure, and there were a large number of pores inside the flocs. When the shear rate gradually increased, the small branches around the floc were more likely to be destroyed. The pores, which had the ability to combine with other particles or clusters, were exposed and filled by the small particles or clusters. Hence, the D_f of the flocs after breakage was higher than those before breakage. This was consistent with a number of other studies [24,30]. This result indicated that the flocs after breakage were more compacted than the clusters formed under the slow stirring rate condition. Moreover, the structures of the flocs were rearranged after breakage.

4.2.3. Influence of shear force on floc size distribution

The variation of floc size distribution at the breakage point under different stirring speeds was plotted on Fig. 4.

This figure showed that floc size distributions stayed nearly the same as the G value increased from 14.9 to 77.5 s^{-1} ; the floc size ranged from about 2–1,700 μm , with the peak observed at about 420 μm . The percentages of the flocs (each with a diameter of

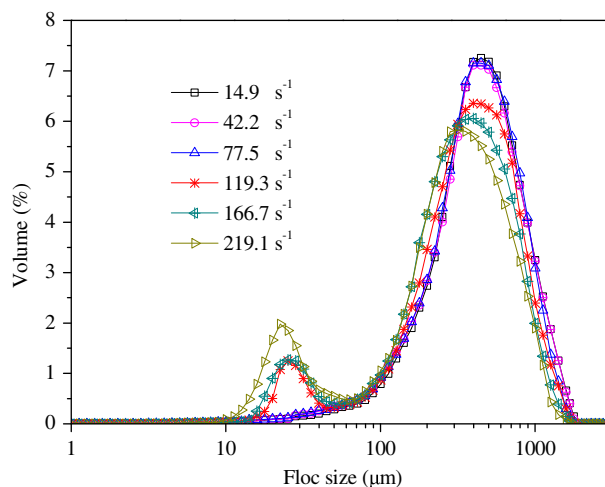


Fig. 4. Variation of floc size distribution after break under various shear forces.

approximately 420 μm) with each G value were 7.17, 7.11, and 7.15%, which were not having any significant differences. When the G value was higher than 119.3 s^{-1} , floc size distribution varied significantly, and a bimodal distribution of floc size was observed. Size distribution peaks are approximately 25 and 370 μm at a G value of 119.3 s^{-1} . At G values of 166.7 and 219.1 s^{-1} , peaks in size distribution were around 23–330 μm , 20–310 μm , respectively.

At the high stirring speed, the peaks in size distribution were much lower than those under low G value conditions. A decreasing trend of larger peaks was observed when the G value was increased from 119.3 to 219.1 s^{-1} . The smaller peak of floc distribution increased with increasing shear rate.

At low G values, the breaking force caused by stirring was lower than the floc's binding force. It was difficult for the agitation to destroy the particles, so the floc size distribution varied little. According to Eq. (28), the breaking force was proportional to the squared G value; thus, the breaking force increased quickly as the stirring speed rose. When the breaking force was larger than the binding force, the weaker binding points among flocs started to break. As a result, the percentage of larger flocs decreased, and a growing number of small particles were discovered.

4.3. Floc strength

In comparing Figs. 2–4, it could be concluded that the floc size, fractal dimension, and size distribution seldom varied when G was below 77.5 s^{-1} . This showed that the flocs could survive during the low stirring rate, and there was little or no floc breakage. However, when the G value increased to 119.3 s^{-1} or above, the floc size decreased dramatically. It was noted that the particle size distribution analyzer could sensitively monitor the variation of floc size. In addition, the fractal dimension and size distribution varied significantly. When G was in the range of 77.5–119.3 s^{-1} , the flocs began to break into small particles. Consequently, a G value of 98.4 s^{-1} (the average G value of 77.5 and 119.3 s^{-1}) was considered to be the critical point of floc breakage in this study.

Once the critical point was determined, the breaking force of fluid and binding force of floc could be calculated according to Eqs. (28) and (29), respectively. Moreover, the binding force coefficient k could also be obtained using Eq. (17). The results indicated that the strength of PAC floc with a dose of 22.5 mg/L was approximately 17.32 nN, and the coefficient of binding force k was about 6.621×10^{-3} . Therefore, the strength

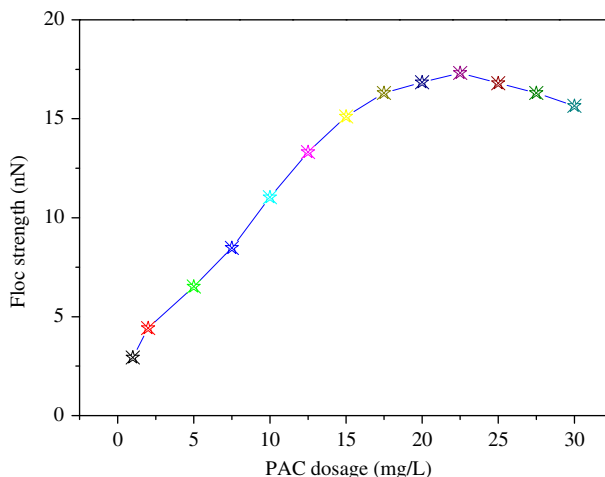


Fig. 5. Variations in floc strength with different PAC doses.

of the floc, which was formed in this study's agitation condition, was:

$$B_f = 6.621 \times 10^{-3} d^{(1+D_f)} \quad (32)$$

Variations in floc strength with different PAC doses under the same agitation condition were evaluated using Eq. (32). The results were shown as Fig. 5. The strength curve exhibited a notable variation at the tested PAC dosage range. At a low dosage of PAC (1–15 mg/L), the floc strength increased significantly. When the PAC dosage was in the range of 17.5–22.5 mg/L, floc strength variation was not obvious (16.31–17.32 nN). However, when PAC dosage increased to above approximately 25 mg/L, a decreasing trend was seen. Therefore, when the coagulant dose was 22.5 mg/L, the flocs had the largest strength, with most efficient turbidity removal.

The explanation for the increased strength of PAC flocs at a low PAC dose could be linked to the increased charge neutralization probability of primary particles. At a low dosage, more and more Al_b species (the main component in PAC) were formed and neutralized the negative charge on colloidal surface with increasing PAC doses [35]. The number of inter-particle bonds within the floc increased as the particles rapidly grew, and the fractal dimension increased with the rise of PAC dose. Consequently, the floc strength significantly increased. When the coagulant dose was increased further, colloids were re-stabilized, resulting from the formation of positively charged particles while the floc size decreased. Moreover, the floc structures were less compact, leading to a lower

fractal dimension. Therefore, floc strength was reduced when the PAC dosage was increased to 25 mg/L or above.

5. Conclusions

This study established a novel quantitative way to evaluate floc strength under turbulent flow conditions by considering binding and breaking forces. Theoretically, the binding force of floc, representing floc strength, was a function of the floc diameter and fractal dimension. The breaking force of fluid was proportional to the squared average velocity gradient and the fourth power of floc diameter.

Floc breakage could be monitored online by the variation of the physical characteristics of flocs in term of floc size, fractal dimension, and size distribution using the particle size distribution analyzer. The physical characteristics did not vary when G was in the range of 14.9–77.5 s⁻¹. However, when G increased to 119.3 s⁻¹ or above, the floc's physical parameters varied significantly.

The critical G value for PAC floc breakage was 98.4 s⁻¹, and the coefficient of binding force k was about 6.621×10^{-3} . The floc strength had an upward trend, followed by a downward trend with the increasing PAC doses. The flocs formed at a PAC dose of 22.5 mg/L were the strongest.

Floc strength, which serves as an indicator of the capacity of flocs to resist shear force, played an important role in determining flocculation performance. This study demonstrates the ability to evaluate floc strength under a given coagulation condition. Thus, not only could floc dynamic behavior be predicted theoretically, but the design of coagulation reactors could be optimized more effectively. This method could also be used to optimize coagulation, and to determine the operational efficiency of the activated sludge in wastewater treatment.

Symbols

B_f	— the binding force of floc (kg m s ⁻²)
A_n	— the net section area at the rupture plane (m ²)
σ	— a constant reflecting average binding strength with respect to the net section area of floc (kg m ⁻¹ s ⁻²)
V_n	— the net volume of a floc (m ³)
d	— floc diameter (m)
α	— the geometry factor ($\alpha = \pi/6$) (–)
e	— the floc porosity (–)
d_e	— the effective diameter (m)
ρ_e	— the floc effective density (kg m ⁻³)

ρ_f	— the density of floc and water, respectively (kg m ⁻³)
ρ_w	— the density of floc and water, respectively (kg m ⁻³)
a	— density function coefficients (kg m ⁻³)
k_p	— density function coefficients (–)
ρ_0	— the density of primary particle (kg m ⁻³)
V_f	— the volume of floc (m ³)
V_w	— the volume of water in floc (m ³)
V_0	— the volume of primary particles in floc (m ³)
M	— the mass of floc (kg)
D_f	— the fractal dimension (–)
k_1	— a coefficient
k_2	— a coefficient
k	— the coefficient of binding force
Δf	— the difference of the pressures between two adjacent points at a small distance (kg m ⁻¹ s ⁻²)
p_1	— the pressures at point 1 (kg m ⁻¹ s ⁻²)
p_2	— the pressures at point 2 (kg m ⁻¹ s ⁻²)
v_1	— the fluctuation velocities of the water at point 1 (ms ⁻¹)
v_2	— the fluctuation velocities of the water at point 2 (ms ⁻¹)
λ	— the Kolmogoroff micro-scale (m)
ν	— the kinematic viscosity (m ² s ⁻¹)
ε	— the mean rate of energy dissipation per unit volume (J m ⁻³ s ⁻¹)
μ	— the absolute viscosity (kg m ⁻¹ s ⁻¹)
β	— the constants, the values is approximately 1
γ	— the constants, the values is approximately 15 ^{-0.5}
F	— the breaking force of fluid (kg m s ⁻²)
G	— the average velocity gradient (s ⁻¹)
P_0	— the impeller power number (–)
N	— the impeller speed (rps)
D	— the impeller diameter (m)
V	— the stirred tank volume (m ³)
Q	— the scatter wave vector
n	— the refractive index of the medium
θ	— the scatter angle
λ_0	— the laser light wavelength in vacuum
I	— the light intensity

References

- [1] J. Sun, L. Qin, G.S. Li, Y. Kang, Effect of hydraulic conditions on flocculation performances and floc characteristics in Chinese herbal extracts by chitosan and chitosan hydrochloride, Chem. Eng. J. 225 (2011) 641–649.
- [2] N. Tambo, Y. Watanabe, Physical aspect of flocculation process—I: Fundamental treatise, Water Res. 13 (1979) 429–439.
- [3] F. Xiao, J.C.H. Huang, B.J. Zhang, C.W. Cui, Effects of low temperature on coagulation kinetics and floc surface morphology using alum, Desalination 237 (2009) 201–213.

- [4] J.J. Ducoste, M.M. Clark, The influence of tank size and impeller geometry on turbulent flocculation: I. Experimental, *Environ. Eng. Sci.* 15 (1998) 215–224.
- [5] P. Jarvis, B. Jefferson, J. Gregory, S.A. Parsons, A review of floc strength and breakage, *Water Res.* 39 (2005) 3121–3137.
- [6] K. McCurdy, K. Carlson, D. Gregory, Floc morphology and cyclic shearing recovery: Comparison of alum and polyaluminum chloride coagulants, *Water Res.* 38 (2004) 486–494.
- [7] W.Z. Yu, J. Gregory, L. Campos, The effect of additional coagulant on the re-growth of alum-kaolin flocs, *Sep. Purif. Technol.* 74 (2010) 305–309.
- [8] J.C. Wei, B.Y. Gao, Q.Y. Yue, Y. Wang, Strength and regrowth properties of polyferric-polymer dual-coagulant flocs in surface water treatment, *J. Hazard. Mater.* 175 (2010) 949–954.
- [9] D.H. Bache, C. Johnson, J.F. McGilligan, E. Rasool, A conceptual view of floc structure in the sweep floc domain, *Water Sci. Technol.* 36 (1997) 49–56.
- [10] T. Li, Z. Zhu, D.S. Wang, C.H. Yao, H.X. Tang, The strength and fractal dimension characteristics of alum-kaolin flocs, *Int. J. Miner. Process.* 82 (2007) 23–29.
- [11] R.J. François, Strength of aluminum hydroxide flocs, *Water Res.* 21 (1987) 1023–1030.
- [12] J. Gregory, Turbidity fluctuations in flowing suspensions, *J. Colloid Interface Sci.* 105 (1985) 357–371.
- [13] M.A. Yukselen, J. Gregory, The reversibility of floc breakage, *Int. J. Miner. Process.* 73 (2004) 251–259.
- [14] D.S. Parker, W.J. Kaufman, D. Jenkins, Floc breakup in turbulent flocculation processes. *J. Sanit. Eng. Div.: Proc. Am. Soc. Civ. Eng.* SA1 (1972) 79–99.
- [15] I.G. Droppo, K. Exall, K. Stafford, Effects of chemical amendments on aquatic floc structure, settling and strength, *Water Res.* 42 (2008) 169–179.
- [16] L. Fabrizi, B. Jefferson, S.A. Parsons, A. Wetherill, P. Jarvis, The role of polymer in improving floc strength for filtration, *Environ. Sci. Technol.* 44 (2010) 6443–6449.
- [17] Y. Yuan, R.R. Farnood, Strength and breakage of activated sludge flocs, *Powder Technol.* 199 (2010) 111–119.
- [18] D.H. Bache, E. Rasol, D. Moffat, F.J. McGilligan, On the strength and character of aluminic-humic flocs, *Water Sci. Technol.* 40 (1999) 81–88.
- [19] Y. Wang, B.Y. Gao, X.M. Xu, W.Y. Xu, G.Y. Xu, Characterization of floc size, strength and structure in various aluminum coagulants treatment, *J. Colloid Interface Sci.* 332 (2009) 354–359.
- [20] W.P. Cheng, P.H. Chen, R.F. Yu, Y.J. Hsieh, Y.W. Huang, Comparing floc strength using a turbidimeter, *Int. J. Miner. Process.* 100 (2011) 142–148.
- [21] R.K. Chakraborti, J.F. Atkinson, J.E. Van Benschoten, Characterization of alum floc by image analysis, *Environ. Sci. Technol.* 34 (2000) 3969–3976.
- [22] P.K. Jin, X.C. Wang, H.X. Chai, Evaluation of floc strength by morphological analysis and PDA online monitoring, *Water Sci. Technol.* 56 (2007) 117–124.
- [23] N. Tambo, H. Hozumi, Physical characteristics of flocs-II: Strength of floc, *Water Res.* 13 (1979) 421–427.
- [24] H.Y. Rong, B.Y. Gao, M. Dong, Y.X. Zhao, S.L. Sun, Y. Wang, Q.Y. Yue, Q. Li, Characterization of size, strength and structure of aluminum-polymer dual-coagulant flocs under different pH and hydraulic conditions, *J. Hazard. Mater.* 252–253 (2013) 330–337.
- [25] D.H. Bache, S.H. Al-Ani, Development of a system for evaluating floc strength, *Water Sci. Technol.* 21 (1989) 529–537.
- [26] N. Tambo, Y. Watanabe, Physical characteristics of flocs—I. The floc density function and aluminium floc, *Water Res.* 13 (1979) 409–419.
- [27] A. Vahedi, B. Gorczyca, Predicting the settling velocity of flocs formed in water treatment using multiple fractal dimensions, *Water Res.* 46 (2012) 4188–4194.
- [28] M. Boller, S. Blaser, Particles under stress, *Water Sci. Technol.* 37 (1998) 9–29.
- [29] J. Bridgeman, B. Jefferson, S. Parsons, Assessing floc strength using CFD to improve organics removal, *Chem. Eng. Res. Des.* 86 (2008) 941–950.
- [30] D.S. Wang, R.B. Wu, Y.Z. Jiang, C.W.K. Chow, Characterization of floc structure and strength: Role of changing shear rates under various coagulation mechanisms, *Colloids Surf., A: Physicochem. Eng. Aspects* 379 (2011) 36–42.
- [31] G.A.C. Ehlers, D. Wagachchi, S.J. Turner, Nutrient conditions and reactor configuration influence floc size distribution and settling properties, *Water Sci. Technol.* 65 (2012) 156–163.
- [32] A. Vahedi, B. Gorczyca, Application of fractal dimensions to study the structure of flocs formed in lime softening process, *Water Res.* 45 (2011) 545–556.
- [33] T.D. Waite, J.K. Cleaver, J.K. Beattie, Aggregation kinetics and fractal structure of γ -alumina assemblies, *J. Colloid Interface Sci.* 241 (2001) 333–339.
- [34] W.Z. Yu, J. Gregory, L. Campos, Breakage and regrowth of al-humic flocs – Effect of additional coagulant dosage, *Environ. Sci. Technol.* 44 (2010) 6371–6376.
- [35] Z.L. Yang, B.Y. Gao, Q.Y. Yue, Coagulation performance and residual aluminum speciation of $Al_2(SO_4)_3$ and polyaluminum chloride (PAC) in Yellow River water treatment, *Chem. Eng. J.* 165 (2010) 122–132.